

StainDiffuser: MultiTask Dual Diffusion Model for Virtual Staining

Tushar Kataria^{1,2}, Beatrice Knudsen³, and Shireen Y. Elhajian^{1,2,4}

¹ Kahlert School of Computing, University of Utah

² Scientific Computing and Imaging Institute, University of Utah

³ Department of Pathology, University of Utah

⁴ Corresponding author

{tushar.kataria,shireen}@sci, beatrice.knudsen@path}.utah.edu

Abstract. Hematoxylin and Eosin (H&E) staining is the most commonly used for disease diagnosis and tumor recurrence tracking. Hematoxylin excels at highlighting nuclei, whereas eosin stains the cytoplasm. However, H&E stain lacks details for differentiating different types of cells relevant to identifying the grade of the disease or response to specific treatment variations. Pathologists require special immunohistochemical (IHC) stains that highlight different cell types. These stains help in accurately identifying different regions of disease growth and their interactions with the cell’s microenvironment. The advent of deep learning models has made Image-to-Image (I2I) translation a key research area, reducing the need for expensive physical staining processes. Pix2Pix and CycleGAN are still the most commonly used methods for virtual staining applications. However, both suffer from hallucinations or staining irregularities when H&E stain has less discriminate information about the underlying cells IHC needs to highlight (e.g., CD3 lymphocytes). Diffusion models are currently the state-of-the-art models for image generation and conditional generation tasks. However, they require extensive and diverse datasets (millions of samples) to converge, which is less feasible for virtual staining applications. Inspired by the success of multitask deep learning models for limited dataset size, we propose StainDiffuser, a novel multitask dual diffusion architecture for virtual staining that converges under a limited training budget. StainDiffuser trains two diffusion processes simultaneously: (a) generation of cell-specific IHC stain from H&E and (b) H&E-based cell segmentation using coarse segmentation only during training. Our results show that StainDiffuser produces high-quality results for easier (CK8/18, epithelial marker) and difficult stains (CD3, Lymphocytes).

Keywords: Virtual Staining · Diffusion Models · Immunohistochemical Staining · Multi-Task Learning · Cycle Consistency

1 Introduction

Hematoxylin and eosin (H&E) stain is commonly used to analyze various tissue samples. Hematoxylin highlights nucleus outlines in the tissue piece and eosin

highlights the cytoplasm. H&E stain is used to make a diagnosis, tracking & re-mission, and treatment planning [17,18]. However, H&E staining does not have all the information that might be required by a pathologist to assess the disease grade or possible response to different treatments [14,15,13]. Pathologists need special immunohistochemical (IHC) stains highlighting different cell types, surfaces, or tumor growth factor markers [15]. IHC stains provide complementary information to H&E stain, and help in making an accurate assessment of the patient’s disease. Conventional methods to obtain these special stains are time-consuming, laborious, and costly [15,19]. Additionally, staining variability across different sites increases the complexity of the analysis [23]. Virtual staining, where deep learning models are used to obtain these special stains, can address all the limitations of traditional methods. Deep learning models require significant training time but less inference time (generally in seconds), reducing the staining time. Trained deep learning models also provide consistently stained patches, thus removing the complexities of stain variations and normalization.

Image-to-Image (I2I) translation models such as Pix2Pix [9] and CycleGAN [29] have consistently shown good performance in generating these virtual stains across different datasets [20,12,27]. These methods have been improved by adding new regularization losses such as structural similarity [27] or augmenting the conditioning generation process by adding or emphasizing complementary edge information [5]. However, all these models tend to have staining irregularities when no marker-specific discriminate features are present in the H&E images [14,5,3]. For example, lymphocyte cells appear indistinguishable from other cells, and tumor growth is not visible to the naked eye in H&E stains [14,5,3]. Since the fundamental cell semantic information and structure are consistent between H&E and IHC stains, IHC specifically accentuates cells through variations in biological/chemical processes, often not visible in H&E-stained images. These models learn to imitate the color distribution –owing to the discriminator and pixel-level loss used during training– and achieve high scores on quantitative metrics such as FID, SSIM, or PSNR. However, they fail to accurately capture the underlying stain distribution. Therefore, there is a need for more exploration of different architectures that minimize staining irregularities.

Diffusion models are the current state of the art in many generations [4] and conditional generation tasks such as inpainting, colorization, and compression [21]. Diffusion models have proven to be very effective in learning the underlying data distributions given sufficient training data and resources. These models have also been used in medical vision tasks such as segmentation [26,25] and generation tasks [7]. MedSegDiff [26] has achieved state-of-the-art performance on the 3D segmentation task. Diffusion Ensembles [25] architecture does segmentation but also uses the diffusion mechanism to provide uncertainty of the model predictions simultaneously. However, diffusion models require large quantities of training data to converge (million samples) to learn the underlying data distribution. They have also been shown to perform subpar on the task of virtual staining where training data are scarce [1].

Multitask deep neural networks have shown better performance than models trained on a single task for low dataset sizes [8,2], where the affinity between the tasks is high. Inspired by this, we propose StainDiffuser, a multitask dual-diffusion model that is designed to simultaneously segment (task 1) the same cells it aims to highlight through virtual staining (task 2), thereby creating an implicit affinity between these tasks. Because of the interaction between segmentation and virtual staining tasks, StainDiffuser, rather than mimicking the color space density, learns discriminate features between different cell types, resulting in more accurate virtual staining performance. Segmentations used for training are obtained via thresholding the DAB channel [11], so no manual annotations are required to train the proposed model. During inference, only the virtual staining diffusion process is used conditioned on H&E, and therefore segmentations are not required at inference. We also propose a variant of a multi-task virtual staining framework that does not require segmentations to be available at training time.

Evaluation of virtual staining models via metrics such as FID score might not be correlated with the accuracy of staining and may be biased towards ImageNet features and network architectures for feature extraction [5,14,22]. Therefore, we report metrics using dinov2 [16] feature space [22] to analyze whether changing encoder feature space better correlates with staining accuracy. To the best of our knowledge, we are the first to comprehensively study conditional diffusion model architectures for virtual staining and quantify the performance of these models using alternative encoder feature space for quantitative metrics. The main contributions of this paper are:-

- Proposed a novel multi-task dual diffusion model for virtual staining where one diffusion process trains to segment the cells and the second to highlight/stain the same cells with IHC marker, regularizing and sharing information through a shared H&E encoder.
- Present comprehensive analysis with qualitative and quantitative results using different encoder feature spaces(inception-net and dinov2[16]).

2 Methods

In this section we explain background material related to diffusion models and the proposed multi-task diffusion model for virtual staining.

Background. The denoising diffusion probabilistic model (DDPM) defines the diffusion process as a two-stage process, i.e., forward and reverse. *Forward process* corrupts the image($\mathbf{I}_0 \in \mathbb{R}^2$) as a Markovian process adding Gaussian noise in T iterations. Gaussian noise is added according to a variance schedule defined by β_1, \dots, β_T . The noisy image at t , denoted by \mathbf{I}_t , can be sampled from the following conditional distribution:

$$q(\mathbf{I}_{t+1}|\mathbf{I}_t) = \mathcal{N}(\mathbf{I}_t; \sqrt{1 - \beta_t}\mathbf{I}_t, \beta_t\mathbb{I}) \quad (1)$$

where \mathbb{I} is the identity matrix. β_t 's are chosen so that after T steps, \mathbf{I}_T is virtually indistinguishable from Gaussian noise. Marginalizing Eq. 1 over t gives the corruption equations at an arbitrary time t :

$$q(\mathbf{I}_t|\mathbf{I}_0) = \mathcal{N}(\mathbf{I}_t; \sqrt{\gamma_t}\mathbf{I}_0, (1 - \gamma_t)\mathbb{I}) \quad (2)$$

where $\gamma_t = \prod_{s=1}^t \beta_s$. This equation gives a closed form solution for sampling of the forward process at an arbitrary time t . This Gaussian re-parameterization also gives a closed form formulation of the posterior distribution of \mathbf{I}_{t-1} given $(\mathbf{I}_0, \mathbf{I}_t)$

$$q(\mathbf{I}_{t-1}|\mathbf{I}_0, \mathbf{I}_t) = \mathcal{N}(\mathbf{I}_{t-1}; \boldsymbol{\mu}, \boldsymbol{\sigma}^2\mathbb{I}) \quad (3)$$

$$\boldsymbol{\mu} = \frac{\sqrt{\gamma_{t-1}}(1 - \beta_t)}{1 - \gamma_t}\mathbf{I}_0 + \frac{\sqrt{\beta_t}(1 - \gamma_{t-1})}{1 - \gamma_t}\mathbf{I}_t, \boldsymbol{\sigma} = \frac{(1 - \gamma_{t-1})(1 - \beta_t)}{(1 - \gamma_{t-1})} \quad (4)$$

Equations 3 and 4 are used during inference to generate images from Gaussian noise. The *reverse process* learns to denoise the noisy image using a deep neural network. A neural network parameterized by θ uses the noisy image and current random noise level $f_\theta(\mathbf{I}_t, \gamma)$ to recover the original image (\mathbf{I}_0) by estimating the noise vector used to corrupt the image. The loss is MSE over estimated noise vs original noise added using equation 2.

$$\mathcal{L} = \mathbb{E}_{\epsilon, t} \{ \|\epsilon - f_\theta(\mathbf{I}_t, t)\|_2 \} \quad (5)$$

In conditional diffusion models, the network, parameterized by θ , is also conditioned on the input image \mathbf{I}_x , resulting in the estimation function defined by $f_\theta(\mathbf{I}_x, \mathbf{I}_t, \gamma)$. In diffusion ensembles [25], the image is concatenated to the noisy image, and in MedSegDiff [26], the encoded representation of the noisy and input image interact via an attention map obtained using Fourier transform of multiscale features. For conditional diffusion models the loss equation is:

$$\mathcal{L} = E_{\epsilon, t} \|\epsilon - f_\theta(\mathbf{I}_x, \mathbf{I}_t, t)\|_2 \quad (6)$$

2.1 StainDiffuser: MultiTask Dual Diffusion Model

Multitask deep neural models have been shown to exceed the performance of models trained on a single task if affinity between the multiple tasks is high [6,10]. These models have also shown better performance than single-task models under data constraint scenarios [8,2]. Even diffusion models trained with multiple tasks have shown good performance in depth prediction [28] and tumor growth prediction [24]. Inspired by the success of multi-task networks, we propose a multi-task diffusion model for virtual staining. The two tasks chosen for the proposed multi-task framework are (a) virtual staining of H&E (generation branch) and (b) H&E cell/object segmentation (segmentation branch). Here, the segmentation task is learning to segment the same cells/objects the virtual stainer is learning to highlight, setting up an implicit affinity between the two

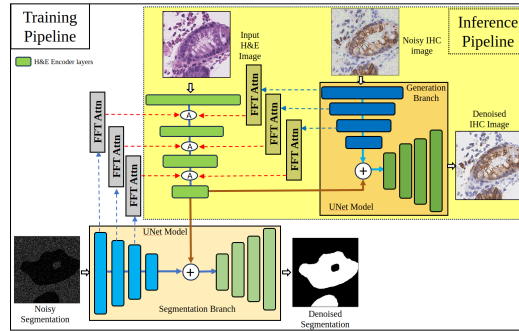


Fig. 1. StainDiffuser: Block diagram of the StainDiffuser model. The generation branch is trained to denoise the noisy IHC and produce a stained patch with correctly highlighted cells. Simultaneously, the segmentation branch is trained to segment the same cells the generation branch needs to highlight. These branches assist each other via the attention framework in the H&E encoder via the FFT based attention. During inference only the generation branch is used to calculate predictions.

tasks. The two branches share information via the input image encoder (H&E), using Fourier attention [26], helping each other in the training process. Using manual segmentation of cells or objects would increase the cost of deploying the model, limiting its’ applicability. To keep the manual annotation cost low, we use coarse segmentations obtained using thresholding and morphological operations [11]. Using automated coarse segmentation removes the manual annotation burden and increases the applicability of the proposed model. Additionally, these segmentations are only used during training, at inference only generation branch is used as shown in Figure 1.

The proposed model consists of two diffusion processes trained simultaneously: (a) segmentation branch and (b) generation branch. The model has an H&E encoder and two UNet⁵ based networks, parameterized by θ and ϕ , for training segmentation and generation diffusion process respectively. We use FFT attention blocks [26] (FFT_{Attn}) at different feature resolutions, where the encoded representation from both diffusion processes attends to features of the H&E image encoder. Let \mathbf{I}_x be the input H&E image, \mathbf{I}_t^{seg} be noisy segmentation image, and \mathbf{I}_t^{ihc} the noisy IHC image given to the segmentation and generation branches, respectively. The segmentation diffusion branch (θ) is trained to minimize the following loss:

$$\mathcal{L}_{seg} = E_{\epsilon, t} \|\epsilon - f_{\theta}(\mathbf{I}_x, \mathbf{I}_t^{seg}, t)\|_2 \quad (7)$$

Similarly, the generation diffusion branch (ϕ) is trained to minimize:

$$\mathcal{L}_{gen} = E_{\epsilon, t} \|\epsilon - f_{\phi}(\mathbf{I}_x, \mathbf{I}_t^{ihc}, t)\|_2 \quad (8)$$

The final loss used to train the full model is obtained by the addition of the above two loss terms $\mathcal{L}_{final} = \mathcal{L}_{gen} + \mathcal{L}_{seg}$.

⁵ Most commonly used architecture for training diffusion models

Without Segmentation Variant. The above architecture needs coarse segmentation that may not be available for different stains. Therefore, to increase the model’s applicability, we propose a multi-task variant that does not depend on segmentation during training, but still leverages the advantages of multi-task training.

For this variant, we remove the segmentation branch from *StainDiffuser*. The two tasks are trained using only the generation branch. The tasks chosen to train the model are (a) H&E to IHC generation and (b) IHC to H&E generation. This model consists of a single input image encoder (alternating between H&E and IHC input) and a single U-Net diffusion model (parameterized by θ) to train both diffusion processes. In the first diffusion process, H&E is the input image to the encoder, and the diffusion process is tasked to denoise the noisy IHC, whereas, in the second diffusion process, the roles of H&E and IHC are switched. Let input H&E and IHC images be defined by \mathbf{I}^{he} and \mathbf{I}^{ihc} , respectively, and noisy H&E and IHC defined by \mathbf{I}_t^{he} and \mathbf{I}_t^{ihc} , respectively. The final loss used to train the model is:

$$\mathcal{L} = E_{\epsilon,t} \|\epsilon - f_{\theta}(\mathbf{I}^{he}, \mathbf{I}_t^{ihc}, t)\|_2 + E_{\epsilon,t} \|\epsilon - f_{\theta}(\mathbf{I}^{ihc}, \mathbf{I}_t^{he}, t)\|_2$$

The implicit cycle consistency (H&E to IHC generation and vice versa) sets up an affinity between the two tasks.

3 Results and Discussion

Datasets. We used two in-house virtual staining datasets for evaluation, H&E to CD3 and H&E to CK8/18. Both the datasets includes H&E whole slide images and corresponding IHC (CK818 or CD3 on the same tissue), from surveillance colonoscopies of 5 patients with active ulcerative colitis. Training patches are sampled from whole slide images (WSI) of 4 patients and last patient WSIs are used for testing. Patch size used for the experiments is equal to 128x128(at 20x) and patches were sampled sequentially with an overlap of 32 pixel size. To limit the sampling of background patches, we only included a patch in training or testing set if at least half of the image has part of the tissue, all other patches are ignored from processing. Sampling procedure ensures we sample enough background that model learns how to perform at tissue boundaries as well. The CK8/18 virtual staining dataset has 49089 paired patches in training and 17407 in testing, whereas CD3 has 51005 and 16622, respectively. The CK8/18 marker highlights epithelial cells, which can be easily identified in H&E, while CD3 marker highlight lymphocytes, which are harder to identify or annotate without referencing an IHC stained slide. CD3 markers are chosen to analyze whether proposed models have the same failure modes as Pix2Pix and CycleGAN.

Evaluation and Implementation Details. We report the Structural Similarity index (SSIM), Signal to Noise Ratio (PSNR), Fréchet Inception Distance (FID), FD, FD_{∞} , Kernel Inception Distance and feature likelihood score (FLS) on the full test set [22]. Inception-Net feature space is used to calculate FID, whereas dinov2 feature space is used to calculate all the other distance metrics

[22]. We ran all our experiments on NVIDIA TITAN V GPU with 12 GB of RAM. Input images of size 64x64 were used for all experiments. Diffusion models were trained using 100 epochs, with number of sampling steps set to 1000.

Baselines. We compare our results both qualitatively and quantitatively with Pix2Pix and CycleGAN. Other conditional diffusion models used for virtual staining did not converge [1], we instead choose MedSegDiff as our diffusion model baseline, where the MedSegDiff model is trained to predict IHC but without any multitask variations proposed. The variant defined in section 2.2 when no segmentations are used is referred as StainDiffuser-wo-seg(or *SDwoS*) in the results section.⁶

Quantitative GAN metrics for CK818 and CD3 virtual staining are shown in Table 1. We can see from the table that StainDiffuser and segmentation variant (mSDwoS) outperforms all other methods for CK818 and CD3 in the FID score and have similar results for PSNR and SSIM. Other metrics FD, FD_{∞} show that diffusion models and StainDiffuser have comparable or less performance than Pix2Pix and CycleGAN models. Various quantitative metrics emphasize the superiority of different models, with a predominant consensus favoring Pix2Pix and CycleGAN.

However, when examined alongside qualitative outcomes, quantitative results fail to align with improved staining performance. In Figure 2, it is evident that StainDiffuser produces the highest quality results for CD3 virtual staining, accurately capturing the majority of lymphocytes. In contrast, both CycleGAN and Pix2Pix exhibit a tendency to under-stain the tissue in most patches. CycleGAN displays heightened sensitivity in staining blood cells, particularly evident in CD3 positive samples (second last column). Both the MedSegDiff and *SDwoS* also struggle to accurately highlight the correct lymphocytes, underscoring the significance of the significance of segmentation diffusion in StainDiffuser. The affinity between the segmentation and virtual staining tasks contributes to the model’s ability to achieve precise and consistent CD3 lymphocyte staining. Additional qualitative results are shown in Supplementary Figure 4.

Table 1. Quantitative Metrics Comparison for both CD3 and CK818 results. We report seven quantitative metrics for both CD3 and CK818 virtual staining results. While the proposed diffusion models outperform Pix2Pix (P2P) and CycleGAN (CG) on certain metrics, they do not consistently excel across all performance metrics. MSD refers to the MedSegDiff baseline.

Datasets	CD3 Results					CK8/18 Results				
	P2P	CG	MSD	SDwoS	StainDiffuser	P2P	CG	MSD	SDwoS	StainDiffuser
PSNR \uparrow	20.717	19.30	19.64	20.21	19.08	23.53	22.28	22.39	22.15	22.43
SSIM \uparrow	0.686	0.646	0.6818	0.671	0.612	0.784	0.762	0.755	0.747	0.774
FID \downarrow	17.405	13.12	32.8783	11.4	18.70	10.26	8.722	6.819	9.305	5.923
FD \downarrow	127.371	127.4	141.21	141.214	141.2	152.7	152.7	171.3	171.32	171.32
FD_{∞} \downarrow	125.801	126.5	141.63	139.507	139.5	151.2	152.4	171.2	169.46	170.53
KID \downarrow	2.06	2.06	2.2909	2.291	2.291	2.18	2.18	2.477	2.478	2.478
FLS \uparrow	140.425	139.9	141.922	150.0	150	138.7	133.9	141.8	143.68	146.22

The results for CK818 stain across all methods are notably high in quality, as depicted in Supplementary Figure 3. However, diffusion models demonstrate

⁶ We will release our code files for public use.

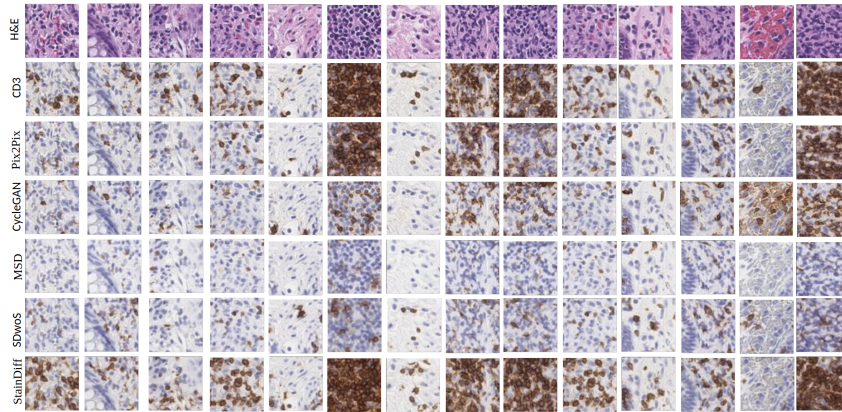


Fig. 2. CD3 Qualitative Results: Comparison of qualitative results using different methods PixPix, CycleGAN, MedSegDiff and proposed dual diffusion methods SDwos and StainDiffuser. The first two rows are original H&E and original CD3 Stain. StainDiffuser shows the best quality results staining higher number of correct CD3 lymphocytes than all other methods. Best viewed after zoom in .

superior performance compared to Pix2Pix and CycleGAN. In Supplementary Figure 3, specifically in columns 6, 7, and 11, both Pix2Pix and CycleGAN exhibit irregularities in properly staining the underlying gland. They miss crucial cell delineation details and only partially stain the gland. Conversely, all diffusion models consistently stain the gland and capture intricate cell details. Furthermore, upon comparing the results of StainDiffuser with other methods, it becomes evident that the proposed model demonstrates less staining variability, consistently and effectively highlighting epithelial cells.

The comparison of quantitative and qualitative results clearly demonstrates a lack of direct correlation between lower quantitative metrics for virtual staining and superior quality outcomes, even when employing distinct encoder representations. Our findings further emphasize that traditional models like Pix2Pix and CycleGAN perform comparably with diffusion models when learning simpler stains with readily available cell-discriminating information in H&E patches. However, it is noteworthy that diffusion-based models such as StainDiffuser excel in delivering better qualitative results, particularly in challenging stains such as CD3 lymphocytes.

4 Conclusion and Future Work

We proposed a novel dual diffusion multi-task model designed for the application of virtual staining. The model employs diffusion processes to learn two conditional image-to-image (I2I) tasks: (a) accurately highlighting or staining the correct cell in immunohistochemistry (IHC), such as lymphocytes in CD3 stain or epithelial cells in CK8/18 stain, and (b) performing segmentation of the same cell or object (e.g., lymphocyte or epithelial segmentation in hematoxylin

and eosin - H&E) simulataneously, thereby establishing an implicit affinity between the two tasks. The multi-task model consistently yields superior results on both straightforward (CK8/18) and challenging virtual staining datasets (CD3), surpassing prior methods across qualitative and quantitative metrics. Our results underscore the lack of correlation between improved performance on GAN quantitative metrics and higher image quality, even when employing a different encoder to compute the latent space representation of generated images. Consequently, in our future research endeavors, we plan to investigate whether any of the GAN metrics proposed in the literature demonstrate a correlation with pathologist evaluations of image quality. Most of our models were trained using a 64x64 patch size. In future work, we aim to scale diffusion models for virtual staining to larger patch sizes and investigate their performance at these extended dimensions.

Acknowledgements

We thank the Department of Pathology, Scientific Computing and Imaging Institute, and the Kahlert School of Computing at the University of Utah for their support of this project.

References

1. Abraham, T.M., Levenson, R.: A comparison of diffusion models and cyclegans for virtual staining of slide-free microscopy images (2023)
2. Bollmann, M., Søgaard, A., Bingel, J.: Multi-task learning for historical text normalization: Size matters. In: Proceedings of the Workshop on Deep Learning Approaches for Low-Resource NLP. pp. 19–24 (2018)
3. Cohen, J.P., Luck, M., Honari, S.: Distribution matching losses can hallucinate features in medical image translation. In: Medical Image Computing and Computer Assisted Intervention–MICCAI 2018: 21st International Conference, Granada, Spain, September 16–20, 2018, Proceedings, Part I. pp. 529–536. Springer (2018)
4. Dhariwal, P., Nichol, A.: Diffusion models beat gans on image synthesis. *Advances in neural information processing systems* **34**, 8780–8794 (2021)
5. Dubey, S., Kataria, T., Knudsen, B., Elhabian, S.Y.: Structural cycle gan for virtual immunohistochemistry staining of gland markers in the colon. In: International Workshop on Machine Learning in Medical Imaging. pp. 447–456. Springer (2023)
6. Fifty, C., Amid, E., Zhao, Z., Yu, T., Anil, R., Finn, C.: Efficiently identifying task groupings for multi-task learning. *Advances in Neural Information Processing Systems* **34**, 27503–27516 (2021)
7. Hung, A.L.Y., Zhao, K., Zheng, H., Yan, R., Raman, S.S., Terzopoulos, D., Sung, K.: Med-cdiff: Conditional medical image generation with diffusion models. *Bio-engineering* **10**(11), 1258 (2023)
8. Ishibashi, H., Higa, K., Furukawa, T.: Multi-task manifold learning for small sample size datasets. *Neurocomputing* **473**, 138–157 (2022)
9. Isola, P., Zhu, J.Y., Zhou, T., Efros, A.A.: Image-to-image translation with conditional adversarial networks. In: Proceedings of the IEEE conference on computer vision and pattern recognition. pp. 1125–1134 (2017)

10. Jiang, J., Chen, B., Pan, J., Wang, X., Liu, D., Jiang, J., Long, M.: Forkmerge: Mitigating negative transfer in auxiliary-task learning. *Advances in Neural Information Processing Systems* **36** (2024)
11. Kataria, T., Rajamani, S., Ayubi, A.B., Bronner, M., Jedrzkiewicz, J., Knudsen, B.S., Elhabian, S.Y.: Automating ground truth annotations for gland segmentation through immunohistochemistry. *Modern Pathology* **36**(12), 100331 (2023)
12. Khan, U., Koivukoski, S., Valkonen, M., Latonen, L., Ruusuvuori, P.: The effect of neural network architecture on virtual h&e staining: Systematic assessment of histological feasibility. *Patterns* **4**(5) (2023)
13. Knudsen, B.S., Zhao, P., Resau, J., Cottingham, S., Gherardi, E., Xu, E., Berghuis, B., Daugherty, J., Grabinski, T., Toro, J., et al.: A novel multipurpose monoclonal antibody for evaluating human c-met expression in preclinical and clinical settings. *Applied Immunohistochemistry & Molecular Morphology* **17**(1), 57–67 (2009)
14. Liu, S., Zhu, C., Xu, F., Jia, X., Shi, Z., Jin, M.: Bci: Breast cancer immunohistochemical image generation through pyramid pix2pix. In: *Proceedings of the IEEE/CVF Conference on Computer Vision and Pattern Recognition*. pp. 1815–1824 (2022)
15. Magaki, S., Hojat, S.A., Wei, B., So, A., Yong, W.H.: An introduction to the performance of immunohistochemistry. *Biobanking: Methods and Protocols* pp. 289–298 (2019)
16. Oquab, M., Darcet, T., Moutakanni, T., Vo, H., Szafraniec, M., Khalidov, V., Fernandez, P., Haziza, D., Massa, F., El-Nouby, A., et al.: Dinov2: Learning robust visual features without supervision. *arXiv preprint arXiv:2304.07193* (2023)
17. Pai, R.K., Lauwers, G.Y., Pai, R.K.: Measuring histologic activity in inflammatory bowel disease: Why and how. *Advances in anatomic pathology* **29**(1), 37–47 (2022)
18. Park, S., Abdi, T., Gentry, M., Laine, L.: Histological disease activity as a predictor of clinical relapse among patients with ulcerative colitis: systematic review and meta-analysis. *Official journal of the American College of Gastroenterology—ACG* **111**(12), 1692–1701 (2016)
19. Rahman, M.A., Sultana, N., Ayman, U., Bhakta, S., Afrose, M., Afrin, M., Haque, Z.: Alcoholic fixation over formalin fixation: A new, safer option for morphologic and molecular analysis of tissues. *Saudi journal of biological sciences* **29**(1), 175–182 (2022)
20. Rivenson, Y., Liu, T., Wei, Z., Zhang, Y., de Haan, K., Ozcan, A.: Phasestain: the digital staining of label-free quantitative phase microscopy images using deep learning. *Light: Science & Applications* **8**(1), 23 (2019)
21. Saharia, C., Chan, W., Chang, H., Lee, C., Ho, J., Salimans, T., Fleet, D., Norouzi, M.: Palette: Image-to-image diffusion models. In: *ACM SIGGRAPH 2022 Conference Proceedings*. pp. 1–10 (2022)
22. Stein, G., Cresswell, J., Hosseinzadeh, R., Sui, Y., Ross, B., Villecroze, V., Liu, Z., Caterini, A.L., Taylor, E., Loaiza-Ganem, G.: Exposing flaws of generative model evaluation metrics and their unfair treatment of diffusion models. *Advances in Neural Information Processing Systems* **36** (2024)
23. Tellez, D., Litjens, G., Bándi, P., Bulten, W., Bokhorst, J.M., Ciompi, F., Van Der Laak, J.: Quantifying the effects of data augmentation and stain color normalization in convolutional neural networks for computational pathology. *Medical image analysis* **58**, 101544 (2019)
24. Wolleb, J., Sandkühler, R., Bieder, F., Cattin, P.C.: The swiss army knife for image-to-image translation: Multi-task diffusion models. *arXiv preprint arXiv:2204.02641* (2022)

25. Wolleb, J., Sandkühler, R., Bieder, F., Valmaggia, P., Cattin, P.C.: Diffusion models for implicit image segmentation ensembles. In: International Conference on Medical Imaging with Deep Learning. pp. 1336–1348. PMLR (2022)
26. Wu, J., Fu, R., Fang, H., Zhang, Y., Yang, Y., Xiong, H., Liu, H., Xu, Y.: Med-segdiff: Medical image segmentation with diffusion probabilistic model. In: Medical Imaging with Deep Learning. pp. 1623–1639. PMLR (2024)
27. Xu, Z., Huang, X., Moro, C.F., Bozóky, B., Zhang, Q.: Gan-based virtual restaining: a promising solution for whole slide image analysis. arXiv preprint arXiv:1901.04059 (2019)
28. Zhou, L., Cui, Z., Xu, C., Zhang, Z., Wang, C., Zhang, T., Yang, J.: Pattern-structure diffusion for multi-task learning. In: Proceedings of the IEEE/CVF Conference on Computer Vision and Pattern Recognition. pp. 4514–4523 (2020)
29. Zhu, J.Y., Park, T., Isola, P., Efros, A.A.: Unpaired image-to-image translation using cycle-consistent adversarial networks. In: Proceedings of the IEEE international conference on computer vision. pp. 2223–2232 (2017)

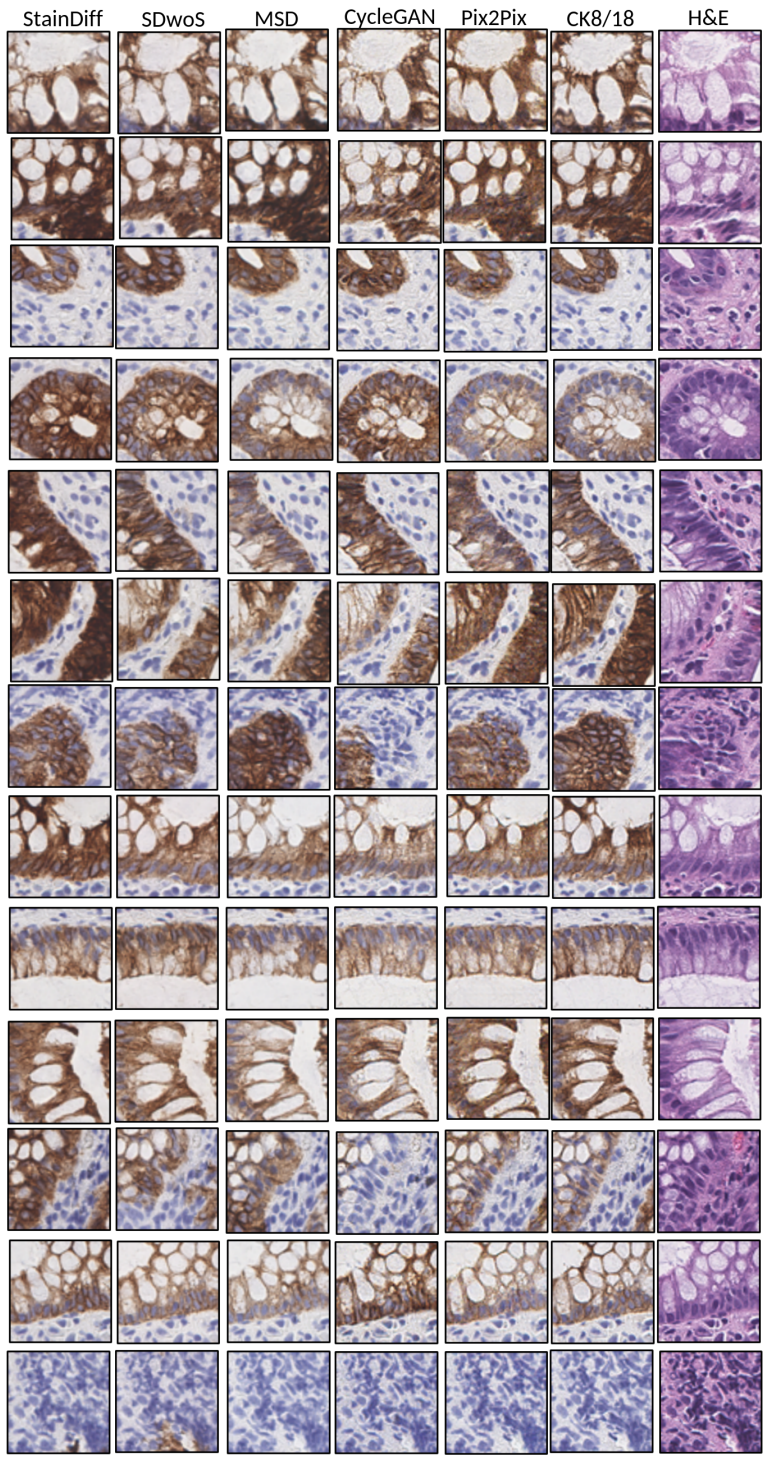


Fig. 3. CK818 Qualitative Results: Comparison of Qualitative result using different methods Pix2Pix, CycleGAN, MedSegDiff and two proposed methods StainDiffuser and SDwoS. First 2 rows are original H&E and original CK8/18 Stain. All diffusion models variants proposed show qualitatively the best results in terms of staining accuracy and cell delineation. Best viewed after zoom in.

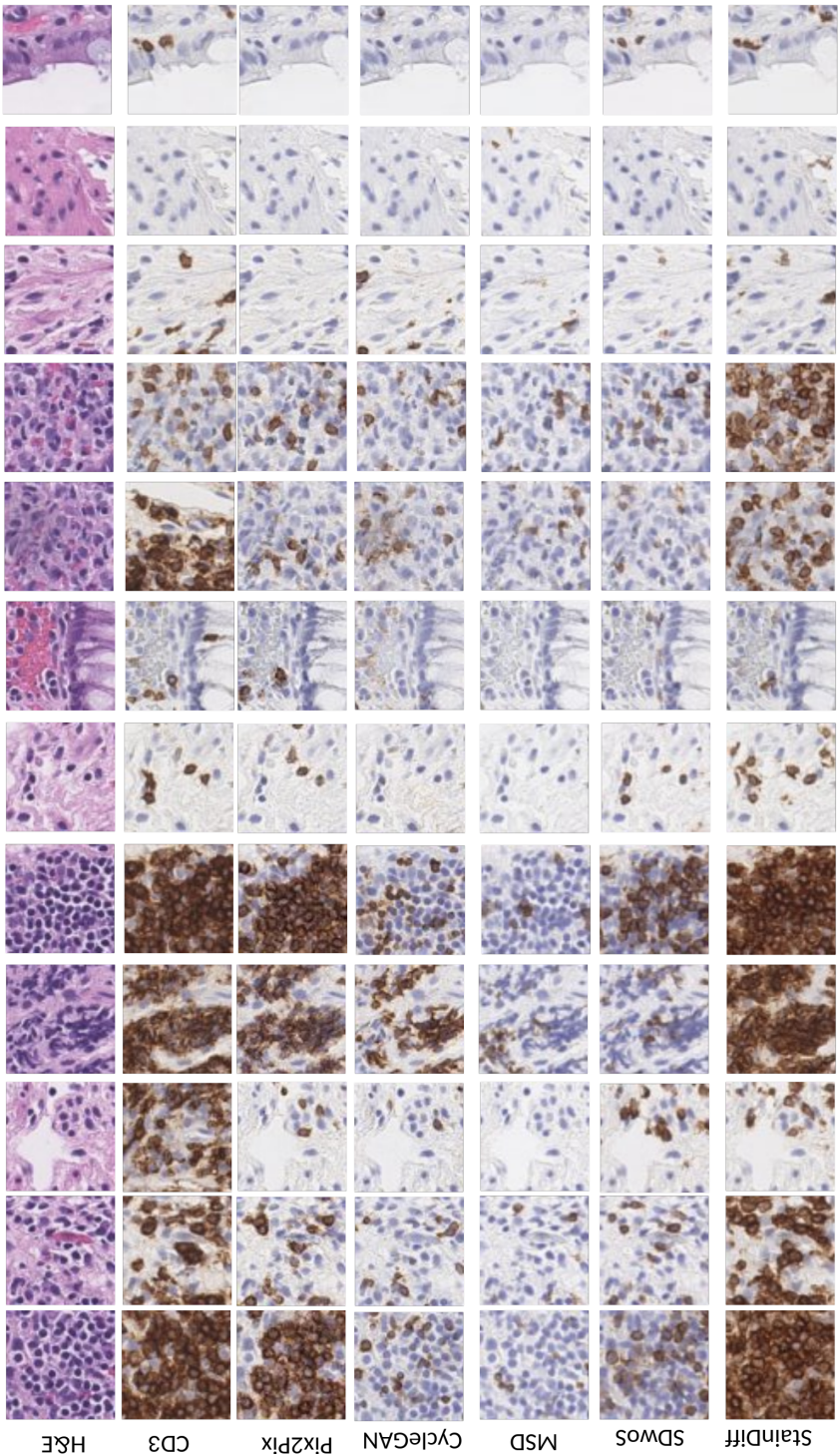


Fig. 4. Additional CD3 Qualitative Results: Comparison of Qualitative result using different methods PixPix, CycleGAN, MedSegDiff and two proposed methods StainDiffuser and SDWoS. First 2 rows are original H&E and original CD3 Stain. All diffusion models variants proposed show qualitatively the best results in terms of staining accuracy and cell delineation. Best viewed after zoom in.